

Article

# Lattice Parameters of Optical Damage Resistant In-Doped LiNbO<sub>3</sub> Crystals

Serguei Sulyanov <sup>1,2</sup> and Tatyana Volk <sup>1,\*</sup>

<sup>1</sup> Shubnikov Institute of Crystallography of FSRC “Crystallography and Photonics” RAS, 119333 Moscow, Russia; sul942@yandex.ru

<sup>2</sup> NRC Kurchatov Institute, Ploshchad’ Akademika Kurchatova, 123098 Moscow, Russia

\* Correspondence: volk@crys.ras.ru

Received: 17 April 2018; Accepted: 3 May 2018; Published: 13 May 2018



**Abstract:** The lattice parameters in optical damage resistant crystal LiNbO<sub>3</sub>-In were measured for the first time using the X-ray powder method with an internal standard, which provides a high accuracy of the results. The lattice parameters vs. In concentration were obtained in the concentration range from 0.24 to 3.2 at % In in the crystal. The results are discussed in the framework of currently accepted model of the LiNbO<sub>3</sub> intrinsic defect structure.

**Keywords:** lithium niobate; structure measurements; optical-damage resistance

## 1. Introduction

Lithium niobate remains one of the basic materials for various optical applications, in particular for nonlinear–optical frequency conversion. The main problem limiting the exploitation of LiNbO<sub>3</sub> in the high-intensity optics is the photoinduced change of refractive indices and birefringence, referred to as “optical damage” or “photorefraction” [1]. Several means have been proposed to reduce this negative effect. The most efficient method is doping with the group of impurities termed “optical-damage resistant” (“ODRI” below); the development of this approach can be found, e.g., in [1]. Presently, this group includes reliably seven ions, namely the divalent Mg [2] and Zn [3], trivalent In [4] and Sc [5] and tetravalent Hf [6], Zr [7] and Sn [8] (this numbering refers to the order of publications).

The similarity in the effects of these impurities on various LiNbO<sub>3</sub> properties, which originates from a common structure reason, allows us to regard them as a “family”. In the framework of the current approach, ODRI doping similarly to an increase of the Li-content serves as a powerful tool for modifying the intrinsic defect structure which controls all practically important LiNbO<sub>3</sub> properties.

Recently, an interest in the ODRI family has revived again due to the encouraging results in LiNbO<sub>3</sub>-Zr crystals, in which a pronounced reduction of the photorefraction occurs at relatively low Zr concentrations (for refs. see the review [9]). The effect is comparable to doping with 4–5 at % Mg. Thus, low Zr concentrations strongly reducing the optical damage, at the same time affect the optical quality to a less degree than high Mg-doping. The approach proposed for the interpretation of Mg (Zn) doping effects, appeared to be not completely adequate for the trivalent and tetravalent ODRI, thus, a refinement of the current model is required. Certain progress is achieved owing to recent studies in ODRI-doped stoichiometric LiNbO<sub>3</sub> (SLN) crystals, e.g., [10,11].

The approach to the intrinsic defect structure discussed below was based on the pioneering X-ray and neutron investigations of the congruently melting LiNbO<sub>3</sub> (CLN) [12–14]. Structure studies in ODRI-doped compositions are few in number. X-ray studies of Mg-doped LiNbO<sub>3</sub> were executed in [15–18]. X-ray and neutron investigations of LiNbO<sub>3</sub>-Zn were performed by us [19–21]; later on, the lattice parameters of LiNbO<sub>3</sub>-Zn were measured in [22]. Recently, in Zr-doped SLN crystals

the lattice parameters vs. Zr concentration were reported [23]. In more detail, these studies will be discussed below comparing them to the results obtained in In-doped LiNbO<sub>3</sub>.

One important comment should be made. As various cations and vacancies can enter both (Li- and Nb-) lattice sites in LiNbO<sub>3</sub>, so the determination of the occupancy and development of a reliable defect structure require a combination of X-ray and neutron studies using powder samples [14,21,24]. This approach provides an advantage of minor extinction problems in powders and better detection of Li with neutrons. Obviously, the reliability of determination of small impurity concentrations demands extremely high accuracy for such experiments. The precise measurements of LiNbO<sub>3</sub>-In lattice parameters presented here are aimed at planned investigations of In-incorporation into the lattice for further studies in the photorefractive and related properties of LiNbO<sub>3</sub>-In, started formerly in [25,26].

Structure measurements in LiNbO<sub>3</sub>-In crystals which are presented here were performed for the first time.

## 2. Results and Discussion

Table 1 and Figure 1a,b show the lattice parameters vs. In concentration in the crystal. The zero points in the curves correspond to the pure (undoped) CLN. Figure 1a presents *a*- and *c*-lattice parameters vs. [In] (in the low-temperature phase LiNbO<sub>3</sub> has R3c space group symmetry), depicted by the triangles and squares, respectively. The quality and uniformity of the crystals deteriorates with the In concentration, so relative errors of In content increase. Figure 1b presents the calculated unit cell volume *V* (the upper curve); for comparison, *V* vs. Zn-concentration is shown (the low dashed curve) calculated from our former measurements in LiNbO<sub>3</sub>-Zn [19].

**Table 1.** Dependence of the lattice parameters on In concentration.

In at % in the Crystal	<i>c</i> , Å	<i>a</i> , Å	<i>V</i> , Å <sup>3</sup>
0	13.86753(6)	5.15054(1)	318.59
0.24	13.86634(17)	5.15117(3)	318.64
0.50	13.86691(14)	5.15185(3)	318.74
1.00	13.86850(14)	5.15338(3)	318.97
1.65	13.87024(11)	5.15606(3)	319.34
2.7	13.87255(11)	5.15887(3)	319.74
3.2	13.87377(9)	5.15956(2)	319.85

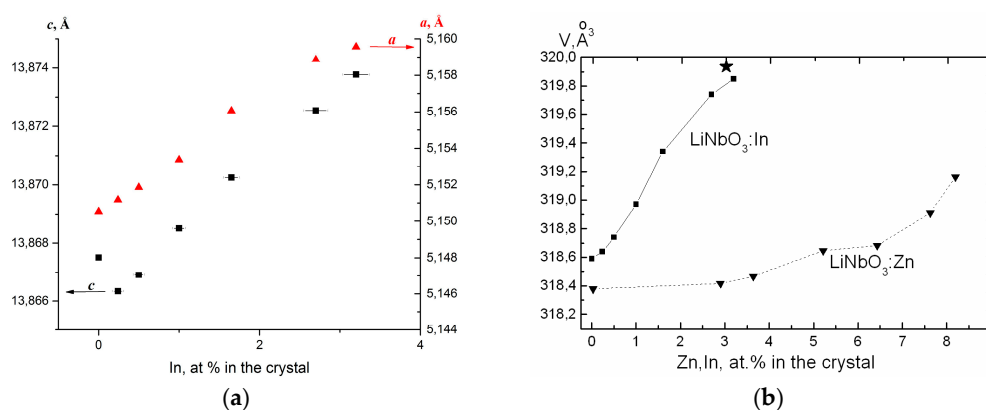


**Figure 1.** (a) Lattice parameters *a* (upper, red triangles) and *c* (lower, black squares with error bars) vs. In concentration in LiNbO<sub>3</sub>-In crystal. (b) Unit-cell volume *V* vs. In (upper) and Zn (lower) concentrations calculated for LiNbO<sub>3</sub>-In and LiNbO<sub>3</sub>-Zn crystals. The curve for LiNbO<sub>3</sub>-Zn is calculated based on the data of [19]. The upper asterisk shows *V* for LiNbO<sub>3</sub>-3% ZrO<sub>2</sub> calculated from [23] (A noncoincidence of the reference points for undoped CLN in the curves for LiNbO<sub>3</sub>-In and LiNbO<sub>3</sub>-Zn is within the experimental error).

To discuss these results, in Table 2 we present the ionic radii  $r_i$  of basic lattice ions and ODRI ions, taken from [27]. As seen,  $\text{In}^{3+}$  and  $\text{Zr}^{4+}$  are the largest ODRI ions. In Figure 1b, in addition to the graphs  $V$  vs.  $\text{In}$  and  $\text{Zn}$  concentrations (the lower and upper curves, respectively), we show the unit-cell volume for  $\text{LiNbO}_3\text{-3\%ZrO}_2$  estimated from the data of [23]. In accordance with Vegard's law, the unit-cell parameters, in particular the unit-cell volume  $V$  smoothly increase with the impurity concentrations, the  $V$  value being noticeably larger for the substitutional impurities having the larger ionic radii ( $\text{In}$  and  $\text{Zr}$ ).

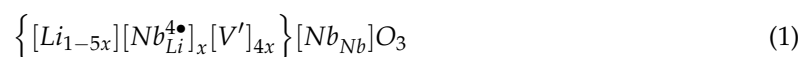
**Table 2.** Ionic radii [27].

Ion	$\text{Li}^+$	$\text{Nb}^{5+}$	$\text{Mg}^{2+}$	$\text{Zn}^{2+}$	$\text{Sc}^{3+}$	$\text{In}^{3+}$	$\text{Zr}^{4+}$	$\text{Hf}^{4+}$
$r_i$ , pm	76	64	72	74	74.5	81	79	71

However, at low  $\text{In}$  concentrations (of 0.25 and 0.5 at %) Vegard's law seems to be violated, since a drop in the parameter  $c$  occurs with respect to this value in the undoped CLN (Figure 1a). At further increase of  $\text{In}$  concentration, the parameter  $c$  steeply grows. Unlike  $c$ , the parameter  $a$  steeply rises starting from the lowest  $\text{In}$  concentrations.

A non-monotonous behavior of  $c$ -parameter at low  $\text{In}$  concentrations is an intriguing feature, since this drop in  $c$  seems to be a common property of ODRI-doped crystals. It was observed in CLN doped with the divalent  $\text{Zn}$  at  $[\text{Zn}] \leq 3$  at % [19] and in SLN doped with the tetravalent  $\text{Zr}$  [23] at  $\text{ZrO}_2$  concentrations of 1.5 and 2.0 mol %. A drop of  $c$  in  $\text{LiNbO}_3\text{-In}$  occurs in a narrow concentration range of 0.5 at % whereas in  $\text{LiNbO}_3\text{-Zn}$  and  $\text{LiNbO}_3\text{-Zr}$  this anomaly is smeared over a range of about 2.5–3% [19,23]. It is reasonable to suggest a common structural origin of these anomalies in the framework of the current model of  $\text{LiNbO}_3$  intrinsic defect structure (the detailed bibliography can be found, e.g., in [1]). To start with, the background of this concept should be considered. In [12–14] it has been found that a part of  $\text{Li}$ -sites in CLN ( $\text{Li}$ -deficient crystals) is occupied by  $\text{Nb}$ -ions. According to [12],  $\text{Nb}$  occupies 4.9% of the  $\text{Li}$ -sites; the later estimate [14] gave a value of about 1%. In the framework of the currently accepted “ $\text{Li}$ -vacancy model” [28], an excess positive charge of  $[\text{Nb}_{\text{Li}}]^{4\bullet}$  is compensated by  $4[\text{V}_{\text{Li}}]'$  (here and below the Kröger–Vink notations are used: a heavy point and a prime denote, respectively, the positive and negative charges with respect to the lattice). The existence of  $\text{Nb}$ -on- $\text{Li}$ -sites (“ $\text{Nb}$ -antisites”) is the cornerstone of the model of  $\text{LiNbO}_3$  intrinsic defect structure.

In the  $\text{Li}$ -vacancy model, the CLN chemical formula is presented by the expression:



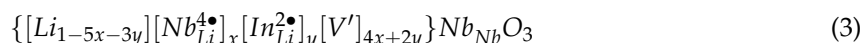
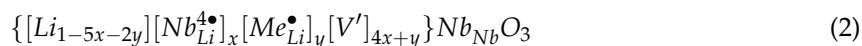
where the group in the braces corresponds to the population of  $\text{Li}$  sites.

The scenario of ODRI incorporation into the  $\text{LiNbO}_3$  lattice (refs. in [1]) is still under debate. Recently, a general consideration of different impurity incorporation into the  $\text{LiNbO}_3$  lattice was presented in [29]. An a priori confidence about ODRI incorporation into the  $\text{Li}$ -sites, at least at low doping was confirmed by numerous experiments. Based on the chemical microanalysis measurements in  $\text{LiNbO}_3\text{-Mg}$  [17,24], it has been concluded that increasing ODRI concentration leads to a gradual removal of  $\text{Nb}$ -antisites, which results in a gradual variation of the crystal properties; the effects are qualitatively similar to increasing  $\text{Li}$ -content. At certain “threshold” concentrations (of 5.5 at %  $\text{Mg}$  and 7 at %  $\text{Zn}$ ), a drastic decrease of photorefraction and step-wise changes of many properties (a shift of the  $\text{OH}$ -vibration absorption band, a kink in the concentration dependences of birefringence, etc. [1]) occur. The structural origin of these thresholds is the most debatable problem. According to the model proposed for the divalent ODRI [30] and supported by the structure measurements in  $\text{LiNbO}_3\text{-Zn}$  [21], the threshold concentration is related to a partial incorporation of ODRI ions into the  $\text{Nb}$ -sites.

An anomaly in the concentration dependence of  $c$ -parameter, discussed in the present work, is observed in the ranges below the thresholds. The threshold concentrations are of 1.7 at %  $\text{In}$  and 7 at %

Zn, respectively, whereas a decreased  $c$  is observed at [In] from 0.25 to 0.5 at % (Figure 1) and [Zn]  $\leq$  3 at % [20]. In Zr-doped crystals, the threshold is of 2 mol % ZrO<sub>2</sub>, while a drop of  $c$  appears at ZrO<sub>2</sub> of about 1.5 mol % ZrO<sub>2</sub> [23].

Let us consider the incorporation of ODRI into LiNbO<sub>3</sub> at concentrations below the thresholds. For clarity, we present the formulas for the divalent Mg and Zn (denoted Me) (2) and trivalent In (3)



where the groups in the brackets correspond to the population of Li sites,  $x$  and  $y$  represent the number of Li-sites occupied by Nb and ODRI, respectively;  $Me_{Li}^{\bullet}$  and  $In_{Li}^{2\bullet}$  denote the divalent (Mg or Zn) and trivalent In ions, respectively, on the Li-sites.

On the basis of precise chemical data, the authors of [17,24] proposed a two-stage scenario of Mg incorporation into LiNbO<sub>3</sub>, according to which at concentrations up to 2–3%, Mg ions remove Nb-antisites, and afterwards, they start to substitute for Li<sub>Li</sub>, forming  $Mg_{Li}^{\bullet}$  compensated by Li-vacancies. The discussed anomalies of lattice parameters in LiNbO<sub>3</sub>-Zn [19] and LiNbO<sub>3</sub>-Zr [23] can be adequately interpreted in the framework of this two-stage scenario. Namely, in LiNbO<sub>3</sub>-Zn a decrease of  $c$  [19] and a plateau in the lattice-cell volume (Figure 1b) below 3% Zn is accounted for by the removal of Nb-antisites, whereas an increase of  $c$  and  $V$  at [Zn] >3% is related to increasing number of Li-vacancies. According to the calculations of [29], Nb-antisites disappear at divalent-impurity concentrations of 3%, which is in excellent agreement with the data for LiNbO<sub>3</sub>-Zn. For the tetravalent ODRI, the calculations of [29] predict the removal of Nb-antisites at concentrations of about 1.6 mol %. A drop of  $c$ -parameter in LiNbO<sub>3</sub>-Zr is observed at [ZrO<sub>2</sub>] of 1.5 and 2.0 mol % [23], which permits us to attribute this anomaly to the removal of Nb-antisites again. Analogously, it would be reasonable to assign a decrease of  $c$ -parameter in LiNbO<sub>3</sub>-In at [In]  $\leq$  0.5 at % (Figure 1a) to the disappearance of Nb<sub>Li</sub>. However, this conclusion disagrees with the calculations of [29], according to which Nb-antisites disappear at the trivalent ODRI concentration of 2.1%. Moreover, based on the IR measurements in LiNbO<sub>3</sub>-Sc, the authors of [31] arrived at the conclusion that Nb-antisites are absent at Sc<sub>2</sub>O<sub>3</sub> > 2 mol %, which agrees with the estimates of [29].

It is important to emphasize that in the framework of the Li-vacancy model, the only reason of a decreased  $c$ -parameter in doped CLN is a decreased content of Nb-antisites. So, the anomaly of  $c$ -parameter at In-concentrations  $\leq$  0.5 at % is related to the removal of Nb-antisites. We now speculate about the reason of why the concentration range of the structure anomaly in LiNbO<sub>3</sub>-In does not conform to the consideration of [29]. The calculations of [30] have shown that for trivalent ions the incorporation into two-cation (Li- and Nb-) sites in LiNbO<sub>3</sub> is energetically favorable since it provides the charge self-compensation; in the case of In-doping it would be presented as  $In_{Li}^{2\bullet}-In_{Nb}^{2\bullet}$ . We suggest that because of the large ionic radius (Table 2), the incorporation of In-ions into the Li-sites is hampered, so they enter both cation sites before the total disappearance of Nb<sub>Li</sub>. In other word, a minimum of  $c$  at low In concentrations can be related to an incomplete removal of Nb-antisites. A distinction from the trivalent Sc<sup>3+</sup> might be caused by the less ionic radius of Sc<sup>3+</sup> (Table 2), which facilitates its incorporation into the Li-site. The specificity of In-doping is indirectly supported by the measurements of IR absorption spectra [25,26] which permitted us to suggest the incorporation of In- ions into both cation sites.

Although this reasoning is too speculative, we believe that an anomaly of the lattice parameter  $c$  observed in low concentration ranges in several ODRI-doped LiNbO<sub>3</sub> originates from a common microscopic reason related to the intrinsic defect structure and is worthy of further investigations.

### 3. Materials and Methods

The crystals were grown by the Czochralski technique from the congruent melt with the ratio [Li]/[Nb] = 0.942. The concentration of In<sub>2</sub>O<sub>3</sub> in the melt was varied from 0.12 to 2 mol %. In this

concentration range the distribution coefficient of In falls down from 1 to 0.8 [32]; in the graphs shown above we present at % In in the crystals. Emphasize that all compositions under study, both undoped and In-doped ones (as well as Zn-doped LiNbO<sub>3</sub> reported by us formerly [3,19–21]) were grown from the same starting charge. An identity in the amount of unintended impurity trace substantiates the reliability of comparisons.

X-ray powder diffraction experiment was performed using X'PERT PRO MRD diffractometer (PANalytical, Almelo, the Netherlands) in the reflection Bragg-Brentano parafocusing geometry (CuK<sub>α</sub> radiation,  $\lambda = 1.5418 \text{ \AA}$ , Ni  $\beta$ -filter). The K<sub>α1</sub> contribution ( $\lambda = 1.5405929 \text{ \AA}$ ) was used further for calculations. We used small pieces of single crystals (about 1 mm<sup>3</sup>) and delicately grinded them between two small sapphire bricks so that not to induce substantial line broadening. We poured a thin layer of the powder of about 10  $\mu\text{m}$  thick onto the standard Si wafer holder which was rotated in its plane during the exposure for better averaging over individual grains. A drop of spirit was used to provide a smoother surface. We used the internal standard method to improve the accuracy of the lattice parameters measurement. Cubic LaB<sub>6</sub> NIST No660a standard was used ( $a = 4.1569162 \pm 0.0000097 \text{ \AA}$  at  $T = 22.5 \text{ }^\circ\text{C}$ ). As is known, this method enables one to make measurements both for the sample and standard actually in the same condition, thus removing possible deviations during the reloading. Our approach was as follows. The powder patterns of a sample-standard mixture were registered within the range of the diffraction angles of  $2\theta = 50\text{--}120^\circ$ . Then, we made the mathematical fitting by pseudo-Voigt functions both for the peaks of LiNbO<sub>3</sub>-In and LaB<sub>6</sub>. Thus, the obtained values of the diffraction angles for the standard were compared with the reference angles. The difference was interpolated by quadratic parabolas. Finally, the initially measured values were corrected mathematically and, to be sure, the obtained Bragg peak positions of LaB<sub>6</sub> were used to calculate the lattice cell parameter by the program DICVOL [33]. Mean absolute angular deviations were within of about  $\Delta 2\theta = 0.0004^\circ$ , which enables one to obtain the cubic cell parameter of the standard with a very good accuracy comparable to that designated in the certificate. Thus, typical accuracy for the cell parameter was  $a = 4.15691(2) \text{ \AA}$ , which is in a very good coincidence with the reference value. Then we used the same correction curves to calculate the Bragg peak positions for LiNbO<sub>3</sub>-In and the obtained values were used to calculate the lattice parameters by the program DICVOL. A typical calculation is presented below in Table 3.

**Table 3.** The DICVOL output for the congruent LiNbO<sub>3</sub> after the Bragg peak position correction.  
DIRECT PARAMETERS:  $a = 5.15054 \text{ \AA}$ ,  $c = 13.86753 \text{ \AA}$ ,  $V = 318.59 \text{ \AA}^3$   
STANDARD DEVIATIONS: 0.00001                      0.00006

H	K	L	DOBS	DCAL	DOBS-DCAL	2TH.OBS	2TH.CAL	DIF.2TH.
2	0	8	1.36867	1.36865	0.00002	68.500	68.501	−0.001
2	2	0	1.28762	1.28764	−0.00002	73.487	73.486	0.001
3	1	2	1.21788	1.21789	−0.00001	78.468	78.468	0.000
2	1	8	1.20857	1.20857	−0.00001	79.191	79.191	0.000
2	0	10	1.17764	1.17766	−0.00002	81.703	81.702	0.001
3	1	4	1.16516	1.16516	0.00000	82.769	82.769	0.000
2	2	6	1.12485	1.12485	0.00002	86.440	86.440	0.000
4	0	2	1.10097	1.10098	−0.00001	88.798	88.797	0.001
2	1	10	1.07099	1.07099	0.00000	91.983	91.983	0.000
4	0	4	1.06157	1.06156	0.00001	93.041	93.042	−0.001
1	1	12	1.05435	1.05434	0.00001	93.872	93.873	−0.001
3	2	2	1.01236	1.01234	0.00001	99.086	99.088	−0.002
4	1	0	0.97335	0.97336	−0.00001	104.630	104.629	0.001
1	0	14	0.96698	0.96698	0.00000	105.613	105.613	0.000
4	0	8	0.93783	0.93783	0.00000	110.442	110.442	0.000
3	0	12	0.91243	0.91243	0.00000	115.178	115.177	0.001
4	1	6	0.89706	0.89706	0.00000	118.340	118.340	0.000

FIGURES OF MERIT: 1.- M(17) = 171.8; 2.- F(17) = 67.3(0.0019, 136).

As seen, the accuracy is quite good and the standard deviations are small.

#### 4. Conclusions

For the first time, the lattice parameters were measured with the very high accuracy in optical-damage-resistant LiNbO<sub>3</sub>-In crystals with In concentrations in the range from 0.12 to 3.2 at % In in the crystal. At [In] ≤ 0.5% the concentration dependence of the parameter *c* is non-monotonous and reveals a drop with respect to the *c*-parameter in undoped LiNbO<sub>3</sub>. Since similar non-monotonous concentration dependence of the *c*-parameter were observed in other ODRI-doped LiNbO<sub>3</sub> crystals (LiNbO<sub>3</sub>-Zn, LiNbO<sub>3</sub>-Zr), a possible common reason is discussed in the framework of the currently accepted model of the intrinsic defect structure of LiNbO<sub>3</sub>.

**Author Contributions:** S.S. performed the X-ray measurements and analyzed the data, T.V. analyzed the data and wrote the paper.

**Acknowledgments:** This work was supported by the Federal Agency of Scientific Organizations (Agreement No. 007-ST/P3363/26). The equipment of the Shared Research Center supported by the Ministry of Education and Science (Project No RFMEFI62114X0005) was used in experiments.

**Conflicts of Interest:** The authors declare no conflict of interest.

#### References

1. Volk, T.; Woehlecke, M. *Lithium Niobate: Defects, Photorefraction and Ferroelectric Switching*; Springer: Berlin/Heidelberg, Germany, 2008; pp. 1–247. ISBN 978-540-70765-3.
2. Zhong, G.G.; Jian, J.; Wu, Z.K. LiNbO<sub>3</sub> doped with MgO. In Proceedings of the 11th IEEE International Conference on Quantum Electronics, Boston, MA, USA, 23–26 June 1980; p. 631.
3. Volk, T.R.; Pryalkin, V.I.; Rubinina, N.M. Optical-damage resistant LiNbO<sub>3</sub>:Zn crystal. *Opt. Lett.* **1990**, *15*, 996–998. [[CrossRef](#)] [[PubMed](#)]
4. Volk, T.R.; Rubinina, N.M. A new optical-damage resistant impurity in LiNbO<sub>3</sub>: Indium. *Ferroelectr. Lett.* **1992**, *14*, 37–43. [[CrossRef](#)]
5. Yamamoto, J.K.; Kitamura, K.; Iyi, N.; Kimura, S.; Furukawa, Y.; Sato, M. Increased optical damage resistance in Sc<sub>2</sub>O<sub>3</sub>-doped LiNbO<sub>3</sub>. *Appl. Phys. Lett.* **1992**, *61*, 2156–2158. [[CrossRef](#)]
6. Kokanyan, E.P.; Razzari, L.; Cristiani, I.; Degiorgio, V.; Gruber, J.B. Reduced photorefraction in hafnium-doped single-domain and periodically poled lithium niobate crystals. *Appl. Phys. Lett.* **2004**, *84*, 1880–1882. [[CrossRef](#)]
7. Kong, Y.; Liu, S.; Zhao, Y.; Liu, H.; Chen, S.; Xu, J. Highly optical damage resistant crystal: Zirconium-oxide-doped lithium niobate. *Appl. Phys. Lett.* **2007**, *91*, 081908. [[CrossRef](#)]
8. Wang, L.; Liu, S.; Kong, Y.; Chen, S.; Huang, Z.; Wu, L.; Rupp, R.; Xu, J. Increased optical-damage resistance in tin-doped lithium niobate. *Opt. Lett.* **2010**, *35*, 883–885. [[CrossRef](#)] [[PubMed](#)]
9. Kong, Y.; Liu, S.; Xu, J.J. Recent advances in the photorefraction of doped lithium niobate crystals. *Materials* **2012**, *5*, 1954–1971. [[CrossRef](#)]
10. Kovács, L.; Szaller, Z.; Lengyel, K.; Corradi, G. Hydroxyl ions in stoichiometric LiNbO<sub>3</sub> crystals doped with optical damage resistant ions. *Opt. Mater.* **2014**, *37*, 55–58. [[CrossRef](#)]
11. Kovács, L.; Szaller, Z.; Lengyel, K.; Péter, Á.; Hajdara, I.; Mandula, G.; Pálfalvi, L.; Hebling, J. Photorefractive damage resistance threshold in stoichiometric LiNbO<sub>3</sub>:Zr crystals. *Opt. Lett.* **2013**, *38*, 2861–2864. [[CrossRef](#)] [[PubMed](#)]
12. Abrahams, S.C.; March, P. Defect structure dependence on composition in lithium niobate. *Acta Crystallogr. Sect. B* **1986**, *42*, 61–68. [[CrossRef](#)]
13. Wilkinson, A.P.; Cheetham, A.K.; Jarman, R.H. The defect structure of congruently melting lithium niobate. *J. Appl. Phys.* **1993**, *74*, 3080–3083. [[CrossRef](#)]
14. Zotov, N.; Boysen, H.; Frey, F.; Metzger, T.; Born, E. Cation substitution models of congruent LiNbO<sub>3</sub> investigated by X-ray and neutron powder diffraction. *J. Phys. Chem. Solids* **1994**, *55*, 145–152. [[CrossRef](#)]
15. Grabmaier, B.C.; Otto, F. Growth and investigation of MgO-doped LiNbO<sub>3</sub>. *J. Cryst. Growth* **1986**, *79*, 682–688. [[CrossRef](#)]

16. Rossner, W.; Grabmaier, B.; Wersing, W. Dielectric high-temperature behaviour of undoped and MgO-doped LiNbO<sub>3</sub> single crystals. *Ferroelectrics* **1989**, *93*, 57–65. [[CrossRef](#)]
17. Grabmaier, B.C.; Wersing, W.; Koestler, W. Properties of undoped and MgO-doped LiNbO<sub>3</sub>; correlation to the defect structure. *J. Cryst. Growth* **1991**, *110*, 339–347. [[CrossRef](#)]
18. Malovichko, G.; Cerclier, O.; Estienne, J.; Grachev, V.; Kokanyan, E.; Boulesteix, C. Lattice constants of K- and Mg-doped LiNbO<sub>3</sub>. Comparison with nonstoichiometric lithium niobate. *J. Phys. Chem. Solids* **1995**, *56*, 1285–1289. [[CrossRef](#)]
19. Abdi, T.; Aillerie, M.; Fontana, M.; Bourson, P.; Volk, T.; Maximov, B.; Sulyanov, S.; Rubinina, N. Influence of Zn doping on electrooptical properties and structure parameters of LiNbO<sub>3</sub>. *Appl. Phys. B* **1999**, *68*, 795–799. [[CrossRef](#)]
20. Volk, T.; Maximov, B.; Chernaya, T.; Rubinina, N.; Woehlecke, M.; Simonov, V. Photorefractive properties of LiNbO<sub>3</sub>:Zn crystals related to the defect structure. *Appl. Phys. B* **2001**, *72*, 647–652. [[CrossRef](#)]
21. Sulyanov, S.; Maximov, B.; Volk, T.; Boysen, H.; Schneider, J.; Rubinina, N.; Hansen, T. Neutron and X-ray study of stoichiometric and doped LiNbO<sub>3</sub>:Zn<sub>0.08</sub>. *Appl. Phys. A* **2002**, *74*, S1031–S1033. [[CrossRef](#)]
22. Chia, C.-T.; Lee, C.-C.; Chang, P.-J.; Hu, M.-L.; Hu, L.J. Substitution mechanism of ZnO-doped lithium niobate crystal determined by powder X-ray diffraction and coercive field. *Appl. Phys. Lett.* **2005**, *86*, 182901. [[CrossRef](#)]
23. Argiolas, N.; Bazzan, M.; Ciampolillo, M.V.; Pozzobon, P.; Sada, C.; Saoner, L.; Zaltron, A.M.; Bacci, L.; Minzioni, P.; Nava, G.; et al. Structural and optical properties of zirconium doped lithium niobate crystals. *J. Appl. Phys.* **2010**, *108*, 093508. [[CrossRef](#)]
24. Iyi, N.; Kitamura, K.; Izumi, F.; Yamamoto, J.K.; Hayashi, T.; Asano, H.; Kimura, S. Comparative study of defect structures in lithium niobate with different compositions. *J. Solid State Chem.* **1992**, *101*, 340–352. [[CrossRef](#)]
25. Volk, T.R.; Woehlecke, M.; Rubinina, N.M.; Razumovskii, N.V.; Jermann, F.; Fischer, C.; Böwer, R. LiNbO<sub>3</sub> with the optical-damage resistant impurity indium. *Appl. Phys. A* **1995**, *60*, 217–225. [[CrossRef](#)]
26. Volk, T.; Woehlecke, M.; Rubinina, N. Optical Damage Resistance in LiNbO<sub>3</sub> Crystals. In *Photorefractive Materials and Their Applications*; Guenter, P., Huignard, J.-P., Eds.; Series in Optical Sciences; Springer: Berlin, Germany, 2006; Volume II, pp. 165–203. ISBN 978-3-540-39135-7.
27. Shannon, R.D.; Prewitt, C.T. Effective ionic radii in oxides and fluorides. *Acta Crystallogr. Sect. B* **1969**, *25*, 925–946. [[CrossRef](#)]
28. Lerner, P.; Legras, C.; Dumas, J.P. Stoechiométrie des monocristaux de métaniobate de lithium. *J. Cryst. Growth* **1968**, *3–4*, 231–235. [[CrossRef](#)]
29. Koyama, C.; Nozawa, J.; Maeda, K.; Fujiwara, K.; Uda, S. Investigation of defect structure of impurity-doped lithium niobate by combining thermodynamic constraints with lattice constant variations. *J. Appl. Phys.* **2015**, *117*, 014102. [[CrossRef](#)]
30. Donnerberg, H.; Tomlinson, S.M.; Catlow, C.R.A.; Schirmer, O.F. Computer-simulation studies of extrinsic defects in LiNbO<sub>3</sub> crystals. *Phys. Rev. B* **1991**, *44*, 4877. [[CrossRef](#)]
31. Shimamura, S.; Watanabe, Y.; Sota, T.; Suzuki, K.; Iyi, N.; Kitamura, K.; Yamazaki, T.; Sugimoto, T.; Yamagishi, K. A defect structure model of LiNbO<sub>3</sub>:Sc<sub>2</sub>O<sub>3</sub>. *J. Phys. Condens. Matter* **1996**, *8*, 6825. [[CrossRef](#)]
32. Kasemir, K.; Betzler, K.; Matzas, B.; Tiegeler, B.; Woehlecke, M.; Gather, B.; Volk, T.; Rubinina, N. Influence of Zn/In codoping on the optical properties of lithium niobate crystals. *J. Appl. Phys.* **1998**, *84*, 5191–5193. [[CrossRef](#)]
33. Boultif, A.; Louër, D. Powder pattern indexing with the dichotomy method. *J. Appl. Crystallogr.* **2004**, *37*, 724–731. [[CrossRef](#)]

